CXCL13 as a Novel Immune Checkpoint for Regulatory B Cells and Its Role in Tumor Metastasis

Jun Ren,*,†,[1] Tianxia Lan,†,[1] Ting Liu,* Yu Liu,† Bin Shao,† Ke Men,† Yu Ma,* Xiao Liang,* Yu-quan Wei,† Min Luo,†,[2] and Xia-wei Wei†,[2]

Tumor metastasis is the primary cause of mortality in patients with cancer. Several chemokines are identified as important mediators of tumor growth and/or metastasis. The level of CXCL13 has been reported to be elevated in serum or tumor tissues in patients, which mainly functions to attract B cells and follicular B helper T cells. However, the role of CXCL13 in cancer growth and metastasis is not fully explored. In the current study, we found that CXCL13 is not a strong mediator to directly promote tumor growth; however, the mice deficient in CXCL13 had far fewer pulmonary metastatic foci than did the wild-type mice in experimental pulmonary metastatic models. In addition, *Cxcl13*$^{-/-}$ mice also had fewer IL-10–producing B cells (CD45^{+}CD19^{+}IL-10^{+}) in the metastatic tumor immune microenvironment than those of wild-type C57BL/6 mice, resulting in an enhanced antitumor immunity. Notably, CXCL13 deficiency further improved the efficacy of a traditional chemotherapeutic drug (cyclophosphamide), as well as that of anti–programmed death receptor-1 immunotherapy. These results suggested that CXCL13 has an important role in regulating IL-10–producing B cells in tumor metastasis and might be a promising target for improving therapeutic efficiency and stimulating tumor immunity in future cancer therapy. *The Journal of Immunology*, **2022, 208: 2425–2435.**

Malignant cancer, such as metastatic melanoma, often metastasizes to distant organs such as lung, liver, or bone marrow, which causes high mortality and is associated with poor prognosis in patients (1). However, the currently available therapies for metastatic cancer only have limited efficacies. Although recent breakthroughs on cancer immunotherapy utilizing anti–programmed death receptor 1 (PD-1) mAb and anti–CTLA-4 mAb have shown encouraging therapeutic effects on advanced melanoma, chemotherapy is still the major therapeutic option. An increasing number of studies have revealed the relevance between tumor metastasis and the tumor immune microenvironment, which consists of immunosuppressive cells, such as regulatory T cells or myeloid-derived suppressor cells. These immune cells might protect metastatic tumor cells from immune surveillance. Notably, chemokines play important regulatory roles in the recruitment of immunosuppressive cells (2). It has been revealed that some types of tumor cells could express the chemokine receptors so that they are able to hijack patients' chemokine networks to achieve migration to distant organs (2). Hence, as a critical regulator of the recruitment and migration of cells, the chemokine network is considered as a crucial mediator of tumor metastasis and malignancy.

Remarkably, CXCL13 and its cognate receptor CXCR5 are associated with lymphoid follicle formation. CXCL13 is a homeostatic chemokine that contributes to the homing and positioning of B cells and follicular helper T cells. CXCR5 is a G protein–coupled receptor that is expressed in B cells and follicular B helper T cells. Many types of tumors could form the ectopic germinal centers in primary lesions or in metastatic sites with the aggregation of B cells. It is conceivable that CXCL13 may participate in tumorigenesis or metastasis by regulating the behaviors of B cells. Recently, it was reported that the deletion of CXCL13 in patients with colorectal tumors is associated with reduced density of B cells in the invasive margin of tumors, which significantly increased the risks of relapse (3). In addition, CXCL13 has been considered as an important marker for the formation of tertiary lymphoid structures (4), whose crucial roles in the maintenance of the immune-responsive tumor microenvironment were recently revealed (5). However, CXCL13 cells were also reported to play protumor roles through regulating the tumor microenvironment (6, 7). In addition, as a subset of the B cell population, regulatory B cells are well known for their capacities to modulate the immune response. It was demonstrated that CXCL13 mediates the migration of regulatory

*Department of Medical Genetics/Prenatal Diagnosis, West China Second Hospital, Sichuan University, Chengdu, Sichuan, People's Republic of China; and †Laboratory of Aging Research and Cancer Drug Target, State Key Laboratory of Biotherapy, National Clinical Research Center for Geriatrics, West China Hospital, Chengdu, Sichuan, People's Republic of China

[1]J.R. and T.L. contributed equally to this work.

[2]M.L. and X.-w.W. contributed equally to this work.

ORCIDs: 0000-0001-6801-516X (J.R.), 0000-0003-0330-7027 (X.L.), 0000-0002-6875-7945 (M.L.), 0000-0002-6513-6422 (X.-w.W.).

Received for publication April 8, 2021. Accepted for publication March 7, 2022.

This work was supported by National Science Fund for Excellent Young Scholars Grant 32122052, National Natural Science Foundation Regional Innovation and Development Grant U19A2003, National Major Scientific and Technological Special Project of China for "Significant New Drugs Development" Grant 2018ZX09733001, Excellent Youth Foundation of the Sichuan Scientific Committee Grant in China 2019JDJQ008, Development Program of China Grant 2016YFA0201402, and by National Natural Science Foundation of China Grant 31800773.

M.L. and X.-w.W. designed the experiments. J.R. and T. Lan conducted the experiments, analyzed the data, and drafted manuscript. T. Liu, Y.L., and B.S. provided technical support for tail vein i.v. injections. K.M., Y.M., and X.L. provided support for multicolor flow cytometry. Y.-q.W. commented on the manuscript and provided helpful discussions.

Address correspondence and reprint requests to Dr. Min Luo and Dr. Xia-wei Wei, Laboratory of Aging Research and Cancer Drug Target, State Key Laboratory of Biotherapy, National Clinical Research Center for Geriatrics, West China Hospital, Sichuan University, No. 17, Block 3, Southern Renmin Road, Chengdu, Sichuan 610041, People's Republic of China. E-mail addresses: minluo_scu@163.com (M.L.) and xiaweiwei@scu.edu.cn (X.-w.W.)

The online version of this article contains supplemental material.

Abbreviations used in this article: CCK-8, Cell Counting Kit-8; CTX, cyclophosphamide; EBI3, EBV-induced gene 3; FCM, flow cytometry; *Grzb*, granzyme B; MHC-II, MHC class II; M2 Mac, type II macrophage; MMP-9, matrix metalloproteinase 9; PD-1, programmed death receptor 1; PD-L1, programmed death ligand 1; *Prfn*, perforin; rmCXCL13, recombinant murine CXCL13; WT, wild-type.

B cells in patients with rheumatoid arthritis (8). Additionally, the immunomodulating capacity of regulatory B cells has been verified in a variety of autoimmune diseases (9), but its roles in oncogenesis and metastasis are still poorly understood. Nevertheless, in breast cancer, a $CD25^+B220^+$ subset of regulatory B cells named tumor-evoked regulatory B cells has been identified (10). Furthermore, in a mouse prostate cancer model, a subset of immunosuppressive plasma cells that are positive for CD138, IL-10, programmed death ligand 1 (PD-L1), and IgA has been identified (11). Importantly, previous studies showed that regulatory B cells or plasma cells play immunosuppressive roles by secreting IL-10, TGF-β1, and PD-L1 (10, 11) However, the role of regulatory B cells in tumor metastasis or chemotherapy resistance is not fully explored.

In this study, we investigated how CXCL13 shapes the tumor microenvironment and influences the antitumor immune response through affecting infiltration of regulatory B cells in tumor metastasis models. We found that $CD19^+IL\text{-}10^+$ regulatory B cells can facilitate tumor metastasis via an IL-10–dependent signaling pathway. We also studied the efficacy of treatment when the knockout of *Cxcl13* was combined with chemotherapy or anti–PD-1 mAb. This study may be of importance to revealing a potential therapy strategy targeting CXCL13 or regulatory B cells for the inhibition or prevention of tumor metastasis.

Materials and Methods

Animals

Cxcl13$^{-/-}$ mice and *Il10*$^{-/-}$ mice were purchased from The Jackson Laboratory. Six- to 8-wk-old wild-type (WT) C57BL/6 mice were purchased from Vital River (Beijing, China). All of these mice were bred in specific pathogen–free conditions. Animal experiments were performed according to the guidelines and approved by the Animal Care and Use Committee of Sichuan University (Chengdu, China).

Cell culture

The murine tumor cell lines B16-F10, LL/2, E.G7-OVA, and ID8 were obtained from the American Typical Culture Collection. B16-F10, LL/2, and ID8 were cultured in DMEM (Life Technologies) with 10% FBS (Life Technologies) and 50 μg/ml penicillin/streptomycin (Life Technologies). E.G7-OVA was maintained in RPMI 1640 medium (Life Technologies) supplemented with 10% FBS, 50 μg/ml penicillin/streptomycin, and another 400 μg/ml G418. All of these cell lines were cultured in 37°C with humidified 5% CO_2.

Cell viability and cell proliferation detection

A Cell Counting Kit-8 (CCK-8; MedChemExpress) was used to test the viabilities of cancer cells according to the manufacturer's protocol. Briefly, different numbers of cells were seeded in 12-well plates and cultured for 24 h before the treatment. Then, the cells were incubated with 500 ng/ml recombinant murine CXCL13 (rmCXCL13) (PeproTech) for indicated times followed by staining with 10% CCK-8 solution at 37°C for another 2 h. Then, the absorbance at 450 nm was measured by a microplate reader.

For cell proliferation assays, tumor cells were seeded into 12-well plates (~2.5×10^4 to 1×10^5 cells per well). After culturing overnight (except E.G7-OVA cells), cells were subsequently cultured in the presence of 500 ng/ml rmCXCL13 and cell numbers were counted every day using a cell counter (Countstar).

Cell migration assay

B16-OVA and LL/2 cells (5×10^4 cells) were suspended in 200 μl of serum-free medium on the upper chamber in the 24-well plates, whereas the lower chamber was filled with 600 μl of medium containing 10% FBS, antibiotics, and 500 ng/ml rmCXCL13. Then, the cells were incubated at 37°C with 5% CO_2 for 24 h. Cells were washed with PBS, fixed with 2% paraformaldehyde for 10 min, stained with 0.5% crystal violet for 5 min at room temperature, and then washed with double-distilled H_2O twice. Finally, cells that remained in the upper chamber were slightly removed using cotton swabs, and those that had migrated to the surface of the lower chamber were captured by a microscope (Olympus). The migrated cells in the images were counted by ImageJ software.

Flow cytometry analysis

The mice under homeostatic conditions or in the experimental pulmonary metastasis models were sacrificed. The lungs containing tumor nodules or not and spleens of mice were collected.

Mouse lung tissues were scissored into small pieces and then digested into a single-cell suspension by 1 mg/ml collagenase type I, 0.5 mg/ml collagenase type IV (Life Technologies), and 0.05 mg/ml DNase I (Sigma-Aldrich) in RPMI 1640 basic medium for 1 h in 37°C. Resulting cell suspensions were passed through 70-μm MACS SmartStrainers (Miltenyi Biotec) to remove clumps of cells and debris. The spleens were directly ground on BD Falcon 70-μm nylon cell strainers with a syringe plunger to obtain single-cell suspensions. RBCs were then lysed by RBC lysis buffer (154 mM NH_4Cl, 10 mM $KHCO_3$, 0.1 mM EDTA 2Na [pH 7.4]) for 5 min at room temperature. Then single cells without RBCs were washed twice with PBS and resuspended in PBS.

For cell surface staining, cells (1×10^6 cells/100 μl/tube) were stained with 1 μl of Abs at 4°C for 30 min in the dark; for intracellular or transcription factor cytokine staining, following the surface staining (2×10^6 cells/100 μl/tube), cells without extra stimulation were performed with a BD Cytofix/Cytoperm fixation/permeabilization kit (BD Bioscience) and transcription factor staining buffer set (eBioscience), respectively. Then, the fixed and permeabilized cells were stained with 5–10 μl of intracellular Abs at room temperature for 2 h. Finally, cells were washed and resuspended in PBS (500 μl/tube), then processed using a FACSCalibur flow cytometer (BD Biosciences) or NovoCyte flow cytometer (ACEA Biosciences), and the results were analyzed using FlowJo version 10 software or NovoExpress software, respectively. Dead cells were excluded using Live/Dead fixable dead cell stain kits (near-infrared fluorescent reactive dye, Life Technologies).

The following anti-mouse Abs purchased from BD Biosciences or BioLegend were used: PerCP-Cyanine5.5– or allophycocyanin-conjugated anti-CD45, PerCP-Cyanine5.5–conjugated anti-CD3ε, allophycocyanin- or PE-conjugated anti-CD4, FITC- or allophycocyanin-conjugated anti-CD8α, PerCP-Cyanine5.5–conjugated anti-CD69, PE-conjugated anti–IFN-γ, allophycocyanin- or PE-conjugated anti-CD19, FITC- or PE-conjugated anti–IL-10, PE-conjugated anti-CD25, Alexa Fluor 488–conjugated anti-Foxp3, PE-conjugated anti-F4/80, FITC-conjugated anti-CD11b, allophycocyanin-conjugated anti-CD11c, PE-conjugated anti–Ly-6G, allophycocyanin-conjugated anti–Ly-6C, Brilliant Violet 421–conjugated anti-CD206, FITC-conjugated anti-CD185 (CXCR5), PE-Cy7–conjugated anti-CD45R/B220, FITC-conjugated anti-CD40, PE-Cy7–conjugated anti–MHC class II (MHC-II), PE-conjugated anti-CD24, Brilliant Violet 421–conjugated anti-CD64, PerCP-Cyanine5.5–conjugated anti-CD21, Alexa Fluor 647–conjugated anti-CD23, FITC-conjugated anti-CD80, FITC-conjugated anti-CD86, FITC-conjugated anti-CD1d, allophycocyanin-conjugated anti-CD5, FITC-conjugated anti-IgM, PE-conjugated anti-IgD, and Brilliant Violet 421–conjugated anti–TGF-β. Allophycocyanin-conjugated anti–arginase-1 was purchased from Invitrogen. PE-conjugated anti–IL-35/EBV-induced gene 3 (EBI3) subunit and Alexa Fluor 488–conjugated anti–IL-35/p35 subunit were purchased from R&D Systems.

Animal experiments

To establish an experimental pulmonary metastatic model, B16-OVA cells (2×10^5) were i.v. injected into C57BL/6 mice. Mice were sacrificed on day 14 or 21 for measuring lung metastatic foci or lung weight. Lung metastatic foci were calculated under a tissue microscope (Leica MZ FLIII). For the s.c. tumor model, B16-OVA cells (1×10^6) were s.c. transplanted into the right back flank of C57BL/6 mice, tumor sizes were measured every 2 d, and tumor volumes were calculated by the following formula: tumor volume = length × weight^2 × 0.52.

For the adoptive transfer B cells model, the lymphocytes were isolated from the spleen of WT or *Il-10*$^{-/-}$ C57BL/6 mice using mouse lymphocyte separation medium (Dakewe Biotech), and the regulatory B cells were stimulated or unstimulated and then separated by a regulatory B cell isolation kit (Miltenyi Biotec) according to the manufacturer's instruction. Briefly, the pre-enrichment of B cells from lymphocytes was stimulated in vitro with 10 μg/ml LPS (Sigma) for 24 h at 37°C with 5% CO_2, and 50 ng/ml PMA and 500 ng/ml ionomycin (Sigma) were added for the last 5 h of stimulation. Then, IL-10–producing regulatory B cells were specifically isolated. B cells from *Il-10*$^{-/-}$ mice were used as a negative control, which were isolated and stimulated in the same way as for the regulatory B cells from WT mice. Subsequently, *Il-10*$^{-/-}$ B cells or regulatory B cells were i.v. adoptively transferred (2×10^6 cells/200 μl/mouse) into tumor-bearing WT recipient mice on days 1, 3, and 6 after the i.v. injection of B16-F10 tumor cells (2×10^5). Mice were sacrificed on day 14 for lung metastases measure, morphological analysis, and flow cytometry (FCM) analysis.

For chemotherapeutics, WT or *Il-10*$^{-/-}$ C57BL/6 mice were i.p. injected with 100 mg/kg cyclophosphamide (CTX; Melonepharma/Meilun Biotech)

or solvent on days 0, 3, and 5 after i.v. injection of B16-F10 tumor cells. For anti–PD-1 (Bio X Cell) therapy, WT or *Il-10*$^{-/-}$ C57BL/6 mice were i.p. injected with control IgG or anti–PD-1 mAbs (250 μg/mouse) at days 0 and 3 after the i.v. injection of B16-F10 tumor cells.

Western blot analysis

Immunoblotting was performed using a standard protocol. After aspirating the supernatant, B16-F10 and LL/2 tumor cells in the plates were lysed and denatured by the addition of sample buffer and boiling for 10 min. Proteins were loaded (10 μl/lane) and resolved by 8% SDS-PAGE and transferred onto polyvinylidene difluoride membranes (Millipore). After blocking with 5% nonfat milk in TBS with 0.05% Tween 20 (TBST) for 1 h at room temperature, the membranes were probed overnight at 4°C with primary Abs used as follows: rabbit polyclonal anti–E-cadherin (Proteintech, 1:5000), rabbit polyclonal anti–N-cadherin (Proteintech, 1:2000), rabbit polyclonal anti–matrix metalloproteinase 9 (MMP-9; Proteintech, 1:1000), and rabbit polyclonal anti-GAPDH (Santa Cruz Biotechnology, 1:4000). After washing with TBST three times, the membranes were incubated with HRP-conjugated goat anti-rabbit secondary Abs for 1 h at room temperature (Cell Signaling Technology, 1:5000). Membranes were then developed using an ECL detection kit (Millipore) and exposed to autoradiography film with a film developer in a dark room. GAPDH was used as an internal control.

Quantitative real-time PCR

Total RNA was extracted by the RNAsimple total RNA kit (Tiangen). Reverse transcription was achieved by iScript reverse transcriptase (Bio-Rad). Real-time PCR was performed with the CFX Connect real-time PCR detection system (Bio-Rad). KAPA SYBR FAST quantitative PCR master mix (Kapa Biosystems) was used, and the expression of the above genes was normalized by 18S rRNA. The mouse primers used were as follows: *Ifng*, 5′-TGAACGCTACACACTG-CATCT-3′ (forward) and 5′-GACTCCTTTTCCGCTTCCTGA-3′ (reverse); perforin (*Prfn*), 5′-TGGAGGTTTTTGTACCAGGC-3′ (forward) and 5′-TAGCC-AATTTTGCAGCTGAG-3′ (reverse); *Tgfb1*, 5′-AAGTTGGCATGGTAGCCC-TT-3′ (forward) and 5′-GGAGAGCCCTGGATACCAAC-3′ (reverse); granzyme B (*Grzb*), 5′-CTCTCGAATAAGGAAGCCCC-3′ (forward) and 5′-CT-GACCTTGTCTCTGGCCTC-3′ (reverse); *Cxcr5*, 5′-ATGAACTACCCACTA-ACCCTGG-3′ (forward) and 5′-TGTAGGGGAATCTCCGTGCT-3′(reverse); 18S rRNA, 5′-CGCCGCTAGAGGTGAAATTCT-3′ (forward) and 5′-CGA-ACCTCCGACTTTCGTTCT-3′ (reverse).

Gelatin zymography analysis for MMP-9 activity

The conditioned media obtained from B16-F10 and LL/2 cells stimulated with or without rmCXCL13 were collected for MMP-9 enzyme activity detection by a gelatin zymography analysis kit according to the manufacturer's protocol (Real-Times (Beijing) Biotechnology). Briefly, serum-free conditioned media samples were subjected to 10% SDS-PAGE, containing 0.1% gelatin under nonreducing conditions. The gels were carefully removed after electrophoresis and washed in renaturing buffer for 30 min at room temperature, and then incubated overnight at 37°C in developing buffer with gentle agitation. After rinsing three times with deionized water, the gels were stained with FastBlue protein staining solution at room temperature. Next, the gels were carefully removed from the water and placed in a plastic sheet protector. A high-resolution scanister was used for scanning the gels. The formation of clear bands at ~100 kDa on the gelatin gels against the blue background indicated the gelatinolytic activity of MMP-9. A collagenase IV lane was added and used as a positive control.

Immunofluorescence staining

Lung specimens were fixed with 4% formaldehyde and embedded in paraffin. Sections (3 μm) were deparaffinized and then subjected to an EDTA buffer for Ag retrieval. The sections were incubated with blocking buffer (5% goat serum) for 30 min at room temperature, and subsequently incubated with secondary Ab (Life Technologies, Alexa Fluor 488 goat anti-mouse IgG, 1:800) for 1 h at room temperature, which was prepared in 1% BSA in PBS. Finally, the cell nucleus was stained with 1 μg/ml DAPI for 5 min at room temperature. Sections were mounted with fluorescent mounting medium (Sigma-Aldrich, F6182) and observed with Vectra 3 automated quantitative pathology imaging system (Akoya Biosciences).

Statistical analysis

Statistical analysis was performed by GraphPad Prism 7 software. The data are presented as mean ± SD or mean ± SEM. The p values were evaluated by a two-sided unpaired t test or one- or two-way ANOVA, in which $p < 0.05$ was considered as statistical significance among each group.

Results

CXCL13 deficiency inhibits murine experimental pulmonary metastasis

Some types of tumor cells express chemokine receptors that subsequently affect tumor growth and metastatic behavior. The cognate receptor of CXCL13, namely, CXCR5, has been reported to be expressed on CT26 cells in vivo and on several pancreatic carcinoma cell lines (A818-4, AsPC1, BxPc3, Colo357, HPAF2, MiaPaCa2, Panc1, Panc89, PancTu-I, and PT45P1) (12). To study how CXCL13–CXCR5 signaling affects tumor metastasis, we first detected the CXCR5 expression in several cell lines, including a murine melanoma cell line (B16-F10), a murine Lewis lung carcinoma cell line (LL/2), a murine lymphoma cell line (E.G7-OVA), and a murine ovarian surface epithelial cell line (ID8). FCM results showed that no CXCR5 was expressed on the cell lines mentioned above or on B16-F10 cells derived from tumor tissues of murine pulmonary metastatic models (in vivo B16-F10) (Fig. 1A). In contrast, as the positive control, mouse lymphocytes highly express CXCR5 (Fig. 1A). Similar results were observed in these cells as further detected by quantitative real-time PCR (Supplemental Fig. 1A).

Next, we managed to study whether CXCL13 could directly influence tumor growth. Results indicated that rmCXCL13-treated tumor cells showed similar viability compared with PBS-treated tumor cells (Fig. 1B). Moreover, our data also showed that CXCL13 does not influence the proliferation of tumor cells (Supplemental Fig. 1B). Collectively, our results demonstrate that CXCL13 does not affect tumor cell growth in vitro, including cell viability and proliferation. To further study whether CXCL13 is associated with tumor growth in vivo, tumor cells including B16-F10 cells, LL/2 cells, or E.G7-OVA cells were injected s.c. into WT or *Cxcl13*$^{-/-}$ mice. However, no significant differences in tumor growth rates of WT and *Cxcl13*$^{-/-}$ mice were observed (Fig. 1C). These results suggested that CXCL13 may not be able to stimulate the growth of tumor cells by CXCL13–CXCR5 signaling in vitro and in vivo. Furthermore, we examined the role of CXCL13 on tumor migration or expression of extracellular matrix remodeling proteins. It was found that exogenous CXCL13 stimulation in vitro does not affect the migration and epithelial-to-mesenchymal transition protein expression of B16-F10 and LL/2 (Supplemental Fig. 2A, 2B). In addition, not only was the protein level of MMP-9 (one of the extracellular matrix remodeling proteins) not affected by CXCL13 stimulation, but also the enzyme activity of MMP-9 did not change (Supplemental Fig. 2C).

In the next set of experiments, we investigated the effects of CXCL13 on tumor metastatic behaviors. To establish the experimental metastasis models, 2×10^5 B16-F10 cells were i.v. injected into WT and *Cxcl13*$^{-/-}$ mice. Remarkably, 14 d after the inoculation of tumor cells, the level of pulmonary metastasis was distinctly lower in *Cxcl13*$^{-/-}$ mice compared to that in WT mice (Fig. 1D). On day 21, the lung weights of *Cxcl13*$^{-/-}$ mice were significantly lower than those of WT mice (Fig. 1E). In addition to melanoma, we also established this kind of model of lung cancer cells, that is, LL/2 cells. After 21 d, mice were sacrificed, and the lungs isolated from *Cxcl13*$^{-/-}$ mice also exhibited lower weights (Fig. 1F). These results showed that pulmonary metastases were inhibited in *Cxcl13*$^{-/-}$ mice and implied that the CXCL13 signaling pathway plays an important role in the process of pulmonary metastasis.

Cxcl13 *deficiency reduced the infiltration of regulatory B cells into the tumor metastatic microenvironment*

The tumor microenvironment contains a wide range of cell types that interact with the complex cytokine/chemokine network. A previous study has shown that the inhibition of chemokine ligand–receptor

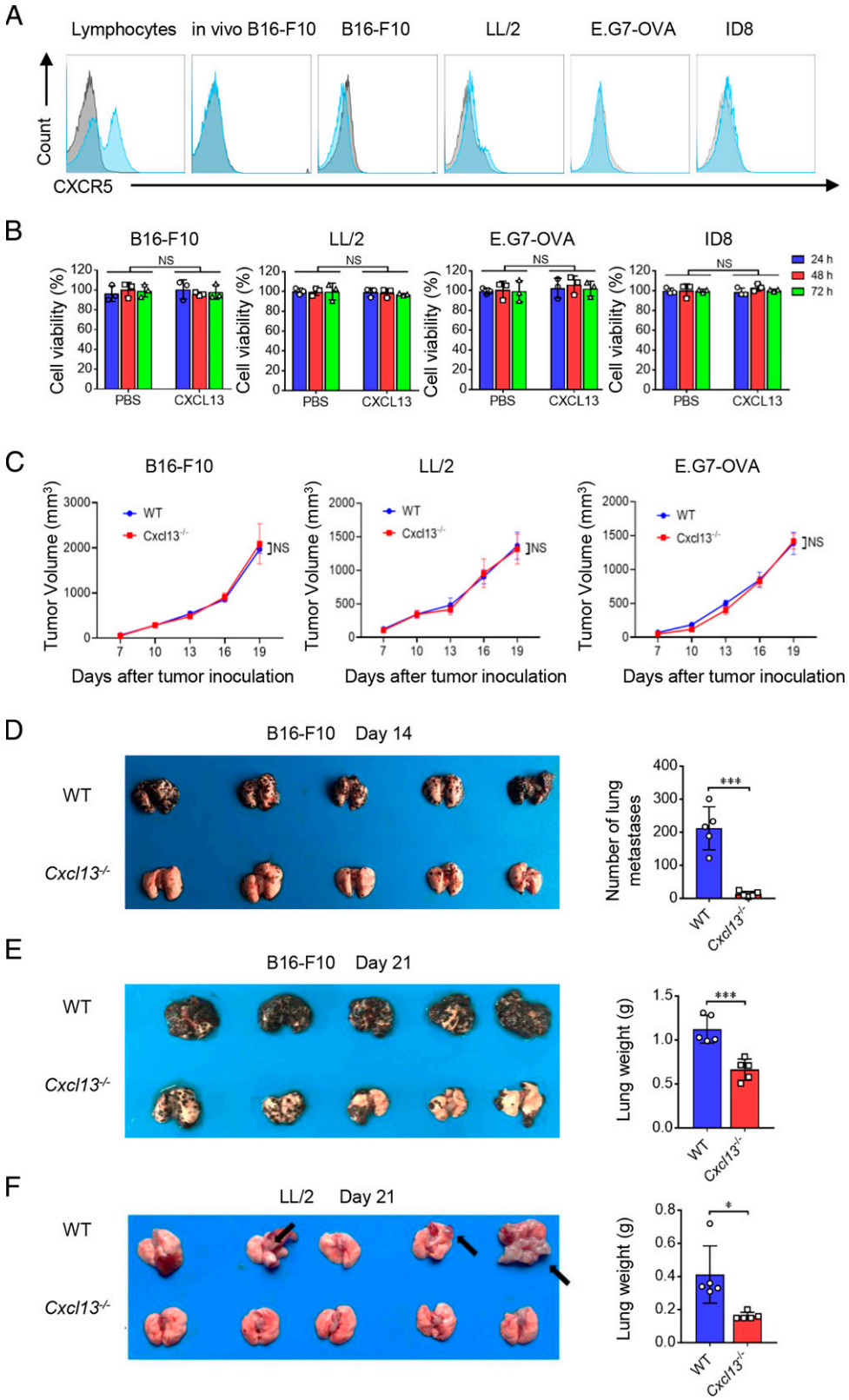

FIGURE 1. *Cxcl13* deficiency inhibits murine experimental pulmonary metastasis. (**A**) The expression levels of CXCR5 in B16-F10, LL/2, E.G7-OVA, and ID8 cell lines were assessed by flow cytometry (FCM). Mouse lymphocytes from the spleen were used as positive control, and the gray area represents the isotype control. (**B**) B16-F10, LL/2, E.G7-OVA, or ID8 cells were treated with 500 ng/ml rmCXCL13 for the indicated times. Cell viability was determined by CCK-8 assays (n = 3 biologically independent samples). (**C**) B16-F10, LL/2, or E.G7-OVA cells (1×10^6) were s.c. transplanted into the right-back flank of wild-type (WT) or *Cxcl13*$^{-/-}$ mice. Tumor volume was monitored at the indicated times (n = 5 mice). (**D**) B16-F10 cells (2×10^5) were i.v. injected into WT or Cxcl13$^{-/-}$ mice to establish experimental pulmonary metastasis models. Mice were sacrificed on day 14 for measuring lung metastases of the tumor. The gross appearance of the lungs (left panel) and the tumor nodules on the lungs (right panel) were examined (n = 5 mice). (**E**) WT or *Cxcl13*$^{-/-}$ mice were injected as in (D). Mice were sacrificed on day 21 for measuring lung weights. The gross appearance of the lungs (left panel) and the lung weights (right panel) were examined (n = 5 mice). (**F**) WT or *Cxcl13*$^{-/-}$ mice were injected with LL/2 cells as in (D). Mice *(Figure legend continues)*

signaling can enhance the migration of T cells to tumor metastatic sites to augment antitumor immunity (13). Moreover, it has been reported that B cells have the capability to secrete immunosuppressive cytokine IL-10, which can repress the T cell–mediated immune response by reducing the secretion of IFN-γ from $CD8^+$ T cells (14).

To see whether CXCL13 could impact immunity against metastatic cancer, we analyzed B cells and IL-10 levels from melanoma pulmonary metastatic sites of WT and *Cxcl13*$^{-/-}$ mice by FCM. Loss of the *Cxcl13* gene led to reduction of the percentages of IL-10–secreting B cells ($CD45^+CD19^+IL\text{-}10^+$) in metastatic sites on days 7, 14, and 21 after tumor cell inoculation (Fig. 2A–F), which suggests that *Cxcl13* deficiency is responsible for the inhibited infiltration of IL-10–secreting B cells at metastatic sites. In addition, the total $CD19^+$ B cell populations on days 14 and 21 slightly declined in *Cxcl13*-deficient mice, which has no statistical significance compared with WT mice (Fig. 2D–F). Furthermore, we investigated the B cell population of WT or *Cxcl13*$^{-/-}$ mice under homeostatic condition. Similar data were observed in the lung, and no difference was found in the proportion of B cells in the spleen (Fig. 2I, 2J).

Generally, regulatory B cells are characterized as a subset of IL-10–secreting B cells. However, previous studies have shown that regulatory B cells also could produce IL-35 and TGF-β to inhibit immune responses (15, 16), in which IL-35 is a heterodimeric cytokine composed of the p35 subunit of IL-12 and the EBI3 subunit of IL-27. As expected, tumor B cells from *Cxcl13*$^{-/-}$ mice dramatically reduced IL-35 and TGF-β production compared with those from WT mice (Fig. 2G, 2H). The above observations support our notion that *Cxcl13* deficiency mainly reduced the infiltration of IL-10–, IL-35–, and TGF-β–secreting regulatory B cells into the tumor metastatic microenvironment.

To uncover the phenotypes of B cells that infiltrated into pulmonary metastatic foci, we gated $CD45^+CD19^+IL\text{-}10^+$ regulatory B cells in metastatic foci by multicolor FCM to analyze the expression of common B cell markers. The data show that this group of B cells is negative for CD23 and expresses low levels of CD21, CD25, CD40, CD80 CD86, and IgM. In addition, they are positive for CD1d and CD5 and express high levels of CD24, MHC-II, and B220/CD45R (Supplemental Fig. 3A). As previous studies revealed, the phenotypes of regulatory B cells in autoimmune diseases or cancer are $CD19^+CD1d^{hi}CD5^+$, $CD21^{hi}CD23^{lo}CD19^+$, or $B220^+CD25^+$ (10, 17, 18). In our study, the regulatory B cells in pulmonary metastasis sites are $CD45^+CD19^+IL\text{-}10^+CD1d^+CD5^+CD24^{hi}MHC\text{-}II^{hi}B220^{hi}$ (Supplemental Fig. 3A), whereas in previous studies, the regulatory B cells identified from autoimmune diseases or cancer were $CD19^+CD1d^{hi}CD5^+$, $CD21^{hi}CD23^{lo}CD19^+$, or $B220^+CD25^+$ (10, 17, 18). To further detect the phenotype of $IL\text{-}10^+$ regulatory B cells in metastasis, we measured the CXCR5 expression and found that loss of *Cxcl13* modestly suppressed the expression of CXCR5 on regulatory B cells (Supplemental Fig. 3B). Therefore, the immunophenotypes of B cells that are responsible for the inhibited metastasis in *Cxcl13*$^{-/-}$ mice in the current study are not completely the same as what previous studies have shown, but they do have some common features.

Furthermore, in the tumor microenvironment, Abs produced by B cells also influence tumor development. Thus, we examined by immunofluorescence whether Ab abundances are changed in *Cxcl13*$^{-/-}$ mice. As expected, *Cxcl13* deficiency enhanced the Ab abundances in the lung metastatic tumor microenvironment (Supplemental Fig. 3C). These data implied that the increase in Abs produced by B cells may also contribute to the antitumor immune response in *Cxcl13*$^{-/-}$ mice, together with the aforementioned reduction in IL-10–, IL-35–, and TGF-β–producing regulatory B cells.

Reduction of regulatory B cell leads to boosted antitumor immunity in the metastatic microenvironment

In the tumor microenvironment, there are some kinds of important immunosuppressive cells such as type II macrophages (M2 Macs), myeloid-derived protumor neutrophils, regulatory T cells, as well as regulatory B cells (19). To understand the mechanism by which CXCL13 influences the metastatic microenvironment, we measured the changes in immune cell percentages at pulmonary metastatic sites in WT and *Cxcl13*$^{-/-}$ mice. We first found that the $CD45^+CD11b^+$ myeloid cell population clearly increased in the *Cxcl13*$^{-/-}$ mice. To further characterize these increased myeloid cell populations, we used Abs against Ly-6G and Ly-6C, respectively, for FCM staining. Data showed that the antitumor monocytes ($CD45^+CD11b^+Ly\text{-}6C^+Ly\text{-}6G^-$) in the tumor metastatic microenvironment were severely elevated, whereas the protumor neutrophils ($CD45^+CD11b^+Ly\text{-}6G^+$) had no visible difference in *Cxcl13*-deficient mice (Fig. 3A, 3B). The above data indicated that the increased $CD45^+CD11b^+$ myeloid cell population was predominantly antitumor monocytes rather than protumor neutrophils. In addition, loss of *Cxcl13* strongly reduced the infiltration of tumor growth–promoting M2 Macs ($CD45^+CD11b^+F4/80^+$ $arginase\text{-}1^+CD206^+$) to the tumor microenvironment (Fig. 3C, 3D). In addition, other types of antitumor immune cells, including dendritic cells ($CD45^+CD11b^+CD11c^+CD24^+CD64^-$) (Fig. 3E, 3F), tumor-infiltrating activated $CD4^+$ T lymphocytes ($CD3^+CD4^+CD69^+$) (Fig. 3G) and $CD8^+$ T lymphocytes ($CD3^+CD8^+CD69^+$) (Fig. 3H), Th17 cells ($CD3^+CD4^+IL\text{-}17A^+$) (Fig. 3I), and CTLs ($CD3^+CD8^+$ $IFN\text{-}\gamma^+$) (Fig. 3J), were found to be increased in metastatic sites. Moreover, in *Cxcl13* knockout mice, the percentages of protumor regulatory T cells ($CD3^+CD4^+Foxp3^+$) decreased compared with those in WT mice (Fig. 3K). Taken together, the FCM data suggested that the reduction of $CD19^+IL\text{-}10^+$ regulatory B cells could lead to the reduction of immunosuppressive cells and thereby enhance the functioning of antitumor cells, which might contribute to the inhibitory effect of pulmonary metastasis observed in *Cxcl13*$^{-/-}$ mice.

Furthermore, we also analyzed the mRNA transcription level of TGF-β (*Tgfb1*), *Prfn*, IFN-γ (*Ifng*), and *Grzb* in pulmonary metastatic foci by quantitative real-time PCR. As an immunomodulating cytokine, the transcription level of *Tgfb1* in *Cxcl13*$^{-/-}$ models is not as strong as that in WT models (Fig. 3L). In addition, the transcription levels of *Prfn*, *Ifng*, and *Grzb* were increased more in *Cxcl13*$^{-/-}$ models than those in WT models (Fig. 3L). Notably, all of these cytokines or functional proteins are associated with cytotoxic T cell activity, which further implies that the loss of CXCL13 could enhance the antitumor immune response in metastatic tumors.

Adoptive transfer of regulatory B cells promotes tumor pulmonary metastasis in WT mice

To further confirm the underlying mechanism and investigate the role of regulatory B cells, adoptive transfer experiments were carried out. Following establishment of the B16-F10 pulmonary metastasis model, *Il-10*$^{-/-}$ B cells or regulatory B cells were i.v. injected into WT tumor-bearing recipient mice. The phenotype of these adoptively transferred B cells was analyzed by FCM, and data indicated that IL-10–secreting

were sacrificed on day 21 for measuring lung weights. The gross appearance of the lungs (left panel) and the lung weights (right panel) were examined (n = 5 mice). Data are presented as mean ± SD or mean ± SEM. Statistical significance was determined by two-way ANOVA or a two-sided unpaired *t* test. $*p < 0.05$, $***p < 0.001$.

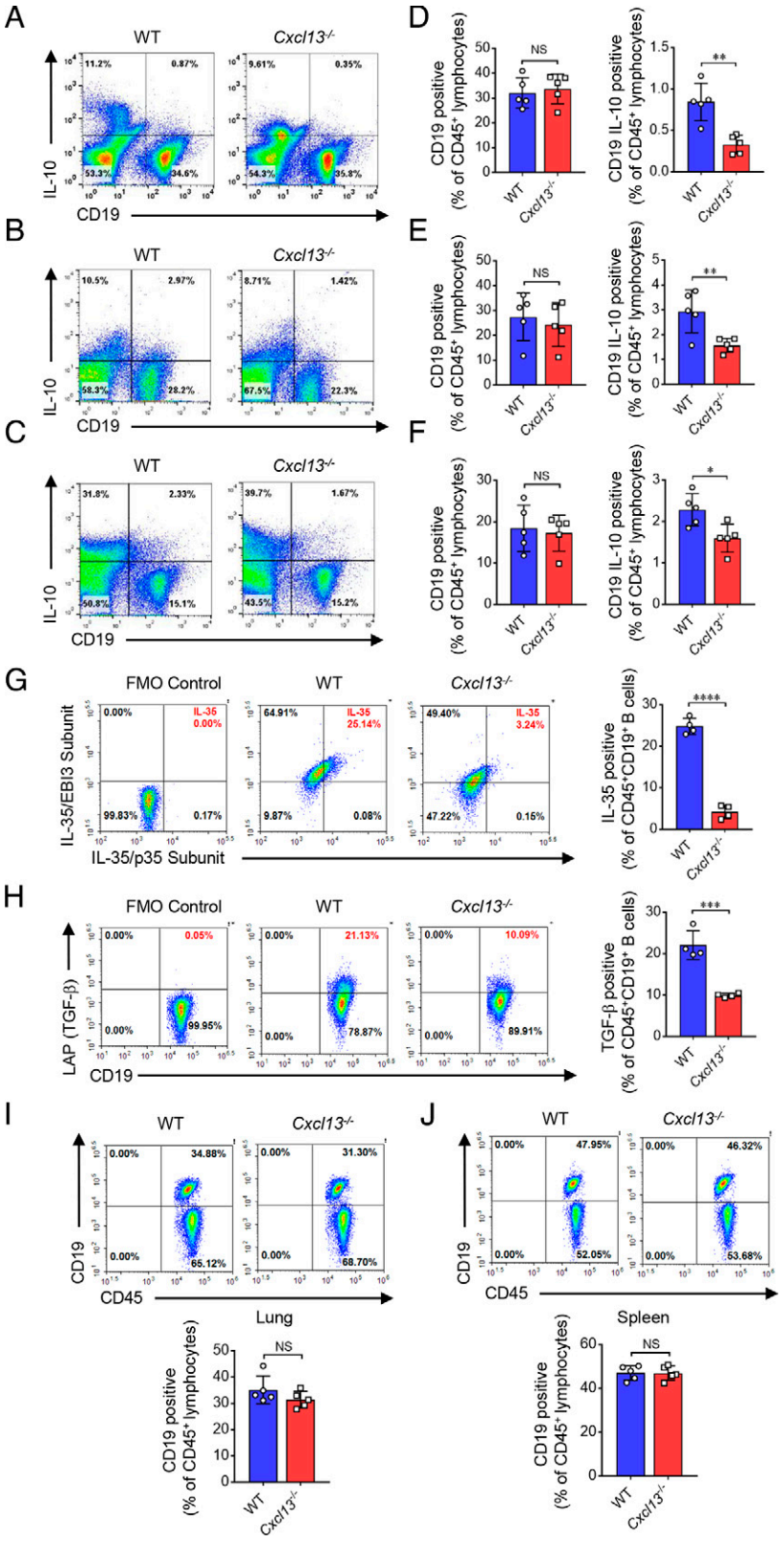

FIGURE 2. CXCL13 deficiency reduced the infiltration of regulatory B cells into the tumor metastatic microenvironment. (**A**–**F**) B16-F10 cells (2×10^5) were i.v. injected into WT or *Cxcl13*$^{-/-}$ mice to establish experimental pulmonary metastasis models. Mice were sacrificed on days 7 (A), 14 (B), and 21 (C) after tumor injection, and then the single-cell suspensions of pulmonary metastatic tumors were prepared and subjected to FCM analysis. Representative scatterplots of the gated CD45$^+$ lymphocytes are shown in (A)–(C). Numbers on the right indicate the percentage of CD19$^+$ B cells producing IL-10 or not in the gated CD45$^+$ lymphocyte population (n = 5 mice). Quantitative data are shown in (D)–(F), respectively. (**G**) Mice were treated in the same way as in (A). Mice were sacrificed on day 14, and single-cell suspensions of pulmonary metastatic tumors were subjected to FCM analysis. Representative scatterplots of the gated CD45$^+$CD19$^+$ B cells are shown in the left panel and are quantified in the right panel. Numbers on the upper right indicate the percentage of IL-35$^+$ B cells (EBI3$^+$P35$^+$) in the gated CD45$^+$CD19$^+$ population. (n = 4 mice). FMO control, fluorescence minus one negative control. (**H**) Single-cell suspension samples were from (G) and subjected to FCM analysis. Representative scatterplots of the gated CD45$^+$CD19$^+$ B cells are shown in the left panel and are quantified in the right panel. Numbers on the upper right indicate the percentage of TGF-β$^+$ B cells in the gated CD45$^+$CD19$^+$ population (n = 4 mice). FMO control, fluorescence minus one negative control. (**I** and **J**) CXCL13 deficiency had no clear effects on the CD19$^+$ B cell population either in the lung (I) or spleen (J) under homeostatic conditions. B cell populations derived from lung or spleen of WT or *Cxcl13*$^{-/-}$ mice were assessed by FCM. Representative scatterplots of the gated CD45$^+$ cells are shown. Numbers on the upper right indicate the percentages of CD19$^+$ B cells in the gated CD45$^+$ population (n = 5 mice). Quantitative data of FCM results are shown in the lower panel. Data are presented as mean ± SD. Statistical significance was determined by a two-sided unpaired *t* test. $*p < 0.05$, $**p < 0.01$, $***p < 0.001$, $****p < 0.0001$.

regulatory B cells were well enriched by the kit from 27 to 84% after in vitro stimulation (Supplemental Fig. 4A). The adoptive transfer results showed that the transfer of IL-10–producing B cells remarkably promoted pulmonary metastasis of B16-F10 cells, whereas the negative control of *Il-10*$^{-/-}$ B cells exhibited minor effects on tumor metastasis compared with the PBS group (Fig. 4A). Additionally, H&E staining further confirmed that adoptive transfer of WT regulatory B cells led to the increased numbers of metastatic foci in lungs (Fig. 4B). We further explored the role of untreated normal B cells in cancer metastasis. However, data indicated that adoptive transfer of unstimulated normal B cells has no effect on tumor pulmonary metastasis (Supplemental Fig. 4B, 4C).

To further investigate how transferred regulatory B cells shaped the tumor microenvironment, the percentages of IL-10–producing B cells,

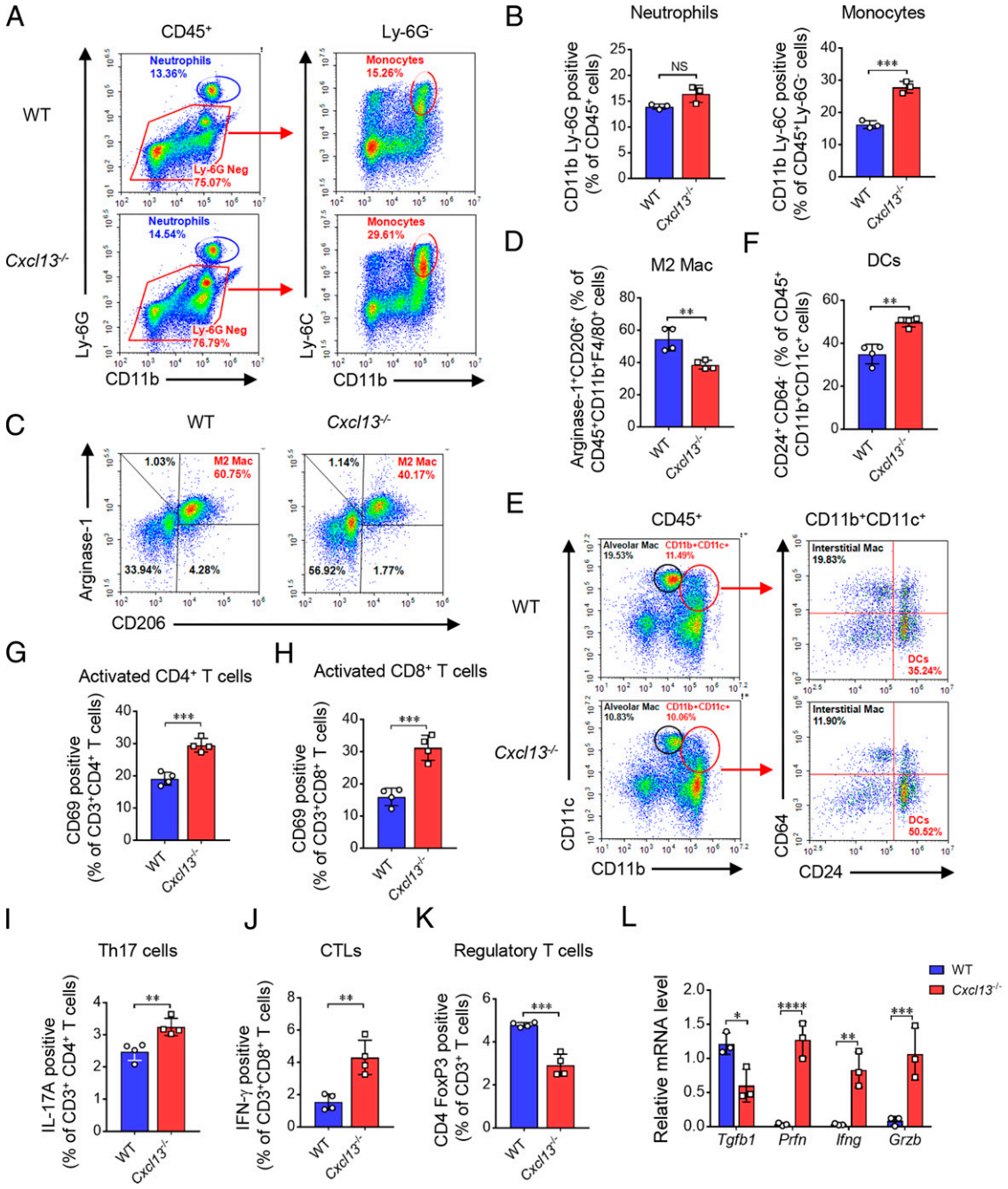

FIGURE 3. Reduction of regulatory B cells leads to boosted antitumor immunity in the metastatic microenvironment. (**A** and **B**) B16-F10 cells (2×10^5) were i.v. injected into WT or *Cxcl13*$^{-/-}$ mice to establish experimental pulmonary metastasis models. Mice were sacrificed on day 14, and the single-cell suspensions of pulmonary metastatic tumors were prepared and subjected to FCM analysis. Representative scatterplots of neutrophils ($CD11b^+Ly\text{-}6G^+$) and monocytes ($CD11b^+Ly\text{-}6C^+Ly\text{-}6G^-$) in the tumor metastatic microenvironment are shown in (A) and quantified in (B). Neutrophils shown on the left panel were gated from the $CD45^+$ subpopulation, and monocytes displayed on the right panel were gated from the $CD45^+Ly\text{-}6G^-$ subpopulation ($n = 3$ mice). (**C** and **D**) Representative scatterplots of M2 Macs ($CD11b^+F4/80^+$arginase-1^+CD206^+) in the tumor metastatic microenvironment are shown in (C) and quantified in (D). Cells were gated from the $CD45^+CD11b^+F4/80^+$ subpopulation ($n = 4$ mice). (**E** and **F**) Representative scatterplots of alveolar macrophages ($CD11b^-CD11c^+$) or dendritic cells (DCs; $CD11b^+CD11c^+CD64^-CD24^+$) in the tumor metastatic microenvironment are shown in (E) and quantified in (F). Cells were gated respectively from $CD45^+$ or $CD45^+CD11b^+CD11c^+$ subpopulations ($n = 4$ mice). (**G**) The percentages of activated $CD4^+$ T cells ($CD4^+CD69^+$) in the tumor metastatic microenvironment were quantified. Cells were gated from the $CD3^+CD4^+$ subpopulation ($n = 4$ mice). (**H**) The percentages of activated $CD8^+$ T cells ($CD8^+CD69^+$) in the tumor metastatic microenvironment were quantified. Cells were gated from the $CD3^+CD8^+$ subpopulation ($n = 4$ mice). (**I**) The percentages of Th17 cells ($CD4^+IL\text{-}17A^+$) in the tumor metastatic microenvironment were quantified. Cells were gated from the $CD3^+CD4^+$ subpopulation ($n = $ I mice). (**J**) Percentages of IFN-γ–producing $CD8^+$ CTLs ($CD8^+IFN\text{-}\gamma^+$) in the tumor metastatic microenvironment were quantified. Cells were gated from the $CD3^+CD8^+$ subpopulation ($n = 4$ mice). (**K**) Percentages of regulatory T cells ($CD4^+Foxp3^+$) in the tumor metastatic microenvironment were quantified. Cells were gated from the $CD3^+$ subpopulation ($n = 4$ mice). (**L**) The mRNA levels of *Tgfb*, *Prfn*, *Ifng*, and *Grzb* in the tumor metastatic environment were assessed by quantitative real-time PCR. Gene expression level was normalized to 18S rRNA ($n = 3$ mice). Data are mean ± SD. Statistical significance was determined by a two-sided unpaired *t* test or two-way ANOVA. $^*p < 0.05$, $^{**}p < 0.01$, $^{***}p < 0.001$, $^{****}p < 0.0001$.

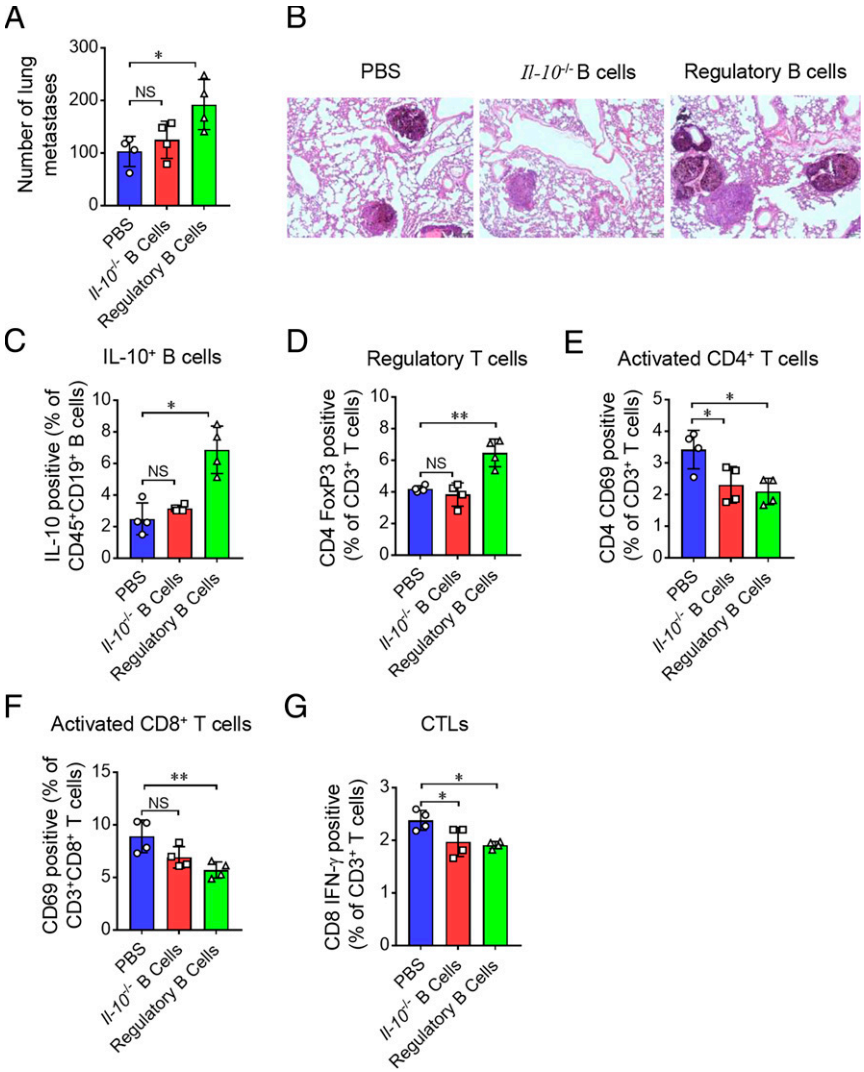

FIGURE 4. Adoptive transfer of regulatory B cells promotes tumor pulmonary metastasis in WT mice. (**A** and **B**) B16-F10 cells (2×10^5) were i.v. injected into WT mice to establish experimental pulmonary metastasis models. Regulatory B cells from WT mice were isolated and stimulated in vitro. Then, they were injected i.v. into recipient mice on days 1, 3, and 6 after tumor cell inoculation (2×10^6 cells/200 μl/mouse). B cells isolated from *Il-10*$^{-/-}$ mice were treated in the same way and used as the negative control. Mice were sacrificed on day 14 for measuring lung metastases of the tumor (A) and lungs were paraffin embedded and stained with H&E (B) (n = 4 mice). Original magnification ×100. (**C**) Single-cell suspensions of pulmonary metastatic tumors from mice in (A) were subjected to FCM analysis. IL-10$^+$ B cells were quantified and plotted as a percentage of CD45$^+$CD19$^+$ B cells (n = 4 mice). (**D**) Regulatory T cells (CD4$^+$Foxp3$^+$) in the tumor metastatic microenvironment were quantified and plotted as the percentage of CD3$^+$ T cells (n = 4 mice). (**E**) Activated CD4$^+$ T cells (CD4$^+$CD69$^+$) in the tumor metastatic microenvironment were quantified and plotted as the percentage of CD3$^+$ T cells (n = 4 mice). (**F**) Activated CD8$^+$ T cells (CD8$^+$CD69$^+$) in the tumor metastatic microenvironment were quantified and plotted as the percentage of CD3$^+$CD8$^+$ T cells (n = 4 mice). (**G**) CTLs (IFN-γ$^+$CD8$^+$) in the tumor metastatic microenvironment were quantified and plotted as the percentage of CD3$^+$ T cells (n = 4 mice). Data are presented as mean ± SD. Statistical significance was determined by one-way ANOVA. *$p < 0.05$, **$p < 0.01$.

regulatory T cells, and activated T cells were detected by FCM. Despite the increased counts of CD45$^+$CD19$^+$IL-10$^+$ B cells in pulmonary metastatic sites after adoptive transfer of regulatory B cells (Fig. 4C), the immune-suppressive CD3$^+$Foxp3$^+$ regulatory T cells were also enriched in metastatic sites when compared with those of the control group (Fig. 4D). In contrast, the percentages of CD4$^+$CD69$^+$ T cells, CD8$^+$CD69$^+$ T cells, and CTLs were reduced after the transfer of regulatory B cells (Fig. 4E–G). Hence, these results demonstrate that regulatory B cells could promote pulmonary metastasis by the secretion of IL-10, which might also be responsible for the increased number of regulatory T cells, the inhibition of CD4$^+$ and CD8$^+$ T cell activation, and downregulation of the IFN-γ level, resulting in a favorable metastatic tumor microenvironment with suppressed antitumor immunity.

Deficiency of CXCL13 enhanced the antitumor efficacy of chemotherapy

It has been revealed that some types of immune cells, including B cells, in the tumor microenvironment contribute to chemotherapy drug resistance (19). To investigate whether CXCL13 is associated with chemoresistance, we treated tumor-bearing *Cxcl13*$^{-/-}$ mice with chemotherapy using CTX. Interestingly, the data showed that both *Cxcl13*$^{-/-}$ mice without chemotherapy and WT mice treated with CTX did not show significant inhibition on tumor metastasis when compared with the control group. However, the effects of chemotherapy in *Cxcl13*$^{-/-}$ mice showed a remarkably decreased number of metastatic foci when compared with other groups (Fig. 5A, 5B). Pathological examination of H&E staining also confirmed these results (Fig. 5C). In addition, FCM analysis revealed significantly elevated percentages of activated CD4$^+$ T cells and CTLs in the CTX-treated *Cxcl13*$^{-/-}$ mice compared with those of other groups (Fig. 5D, 5E). In conclusion, these results demonstrated that CXCL13 might be closely associated with chemoresistance and is a potential target for enhancing the antitumor effects of chemotherapy with a combinational therapeutic strategy.

Deficiency of CXCL13 enhanced the efficacy of cancer immunotherapy targeting PD-1

So far, targeted therapy against immune checkpoints has been intensively studied, such as targeting PD-1 and CTLA-4 in the treatment of melanoma and non–small cell lung carcinoma (20). It has been proven that pembrolizumab (an anti–PD-1 Ab) could prolong progression-free and overall survival of patients with melanoma (21, 22). However, immunotherapy targeting PD-1 is still sometimes limited by the tumor microenvironment. In the current study, we investigated whether CXCL13 and regulatory B cells affect the antitumor effects of immune checkpoint–targeted therapy. mAbs against PD-1 were injected into *Cxcl13*$^{-/-}$ mice, and WT mice were inoculated with B16-F10 melanoma cells. The data showed that, although mAbs against PD-1 were effective in the treatment of melanoma pulmonary metastasis in WT mice, the *Cxcl13*$^{-/-}$ mice manifested

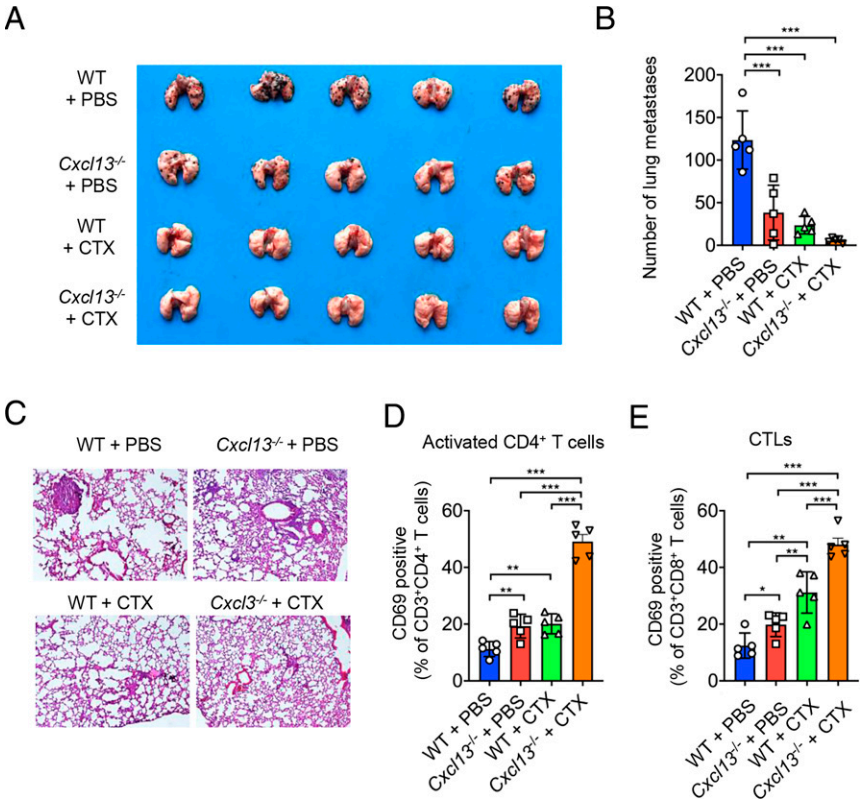

FIGURE 5. CXCL13 deficiency enhanced the metastasis inhibitory ability of chemotherapy. (**A**) CTX was dissolved in sterilized PBS. WT and *Cxcl113*$^{-/-}$ mice in treatment groups were i.p. administered with CTX (100 mg/kg body weight in 0.2 ml of saline/mouse) on days 3 and 6 following i.v. injection of B16-F10 cells (2×10^5). WT and *Cxcl113*$^{-/-}$ mice in control groups were i.p. administered with the same volume of sterilized PBS at the same time points. All mice were sacrificed on day 14, and the gross appearance of the lungs was examined (n = 5 mice). (**B** and **C**) Lungs from WT and *Cxcl113*$^{-/-}$ mice in (A) were isolated for measuring lung metastases of the tumor (B) and lungs were paraffin embedded and stained with H&E (C) (n = 5 mice). Original magnification ×100. (**D**) Single-cell suspensions of pulmonary metastatic tumors from mice in (A) were subjected to FCM analysis. Activated CD4$^+$ T cells (CD4$^+$CD69$^+$) in the tumor metastatic microenvironment were quantified and plotted as a percentage of CD3$^+$CD4$^+$ T cells (n = 5 mice). (**E**) IFN-γ$^+$CD8$^+$ T cells in the tumor metastatic microenvironment were quantified and plotted as a percentage of CD3$^+$CD8$^+$ T cells (n = 5 mice). Data are presented as mean ± SD. Statistical significance was determined by one-way ANOVA. $*p < 0.05$, $**p < 0.01$, $***p < 0.001$.

better outcomes (Fig. 6A, 6B). However, the most favorable outcomes were observed in Cxcl13$^{-/-}$ mice treated with mAbs against PD-1 (Fig. 6A, 6B). Moreover, the results from H&E staining analysis also suggested that the mAbs against PD-1 are more effective for the treatment of melanoma pulmonary metastasis in *Cxcl13*$^{-/-}$ mice than that in WT mice (Fig. 6C). The results showed that more activated CD4$^+$ T cells and CTLs were observed in the *Cxcl13*$^{-/-}$ plus anti–PD-1 mAb group (Fig. 6D, 6E). These results indicate that the mAbs against PD-1 are more effective for the augmentation of T cell responses in *Cxcl13*$^{-/-}$ mice than that in WT mice. In addition, compared to the control group, anti–PD-1 Abs made no significant difference between the proportion of CD4$^+$Foxp3$^+$ regulatory T cells in the metastatic sites of WT mice, but they led to decreased regulatory T cells in the metastatic sites of *Cxcl13*$^{-/-}$ mice (Fig. 6F). In conclusion, our study shows that mAbs against PD-1 are more effective for the treatment of melanoma pulmonary metastasis in *Cxcl13*$^{-/-}$ mice than in WT mice, which implies that CXCL13 may be considered as an combinational therapeutic target for enhancing the efficacy of immune checkpoint inhibitors in the treatment of pulmonary metastatic tumors.

Discussion

Tumor metastasis is the primary cause of mortality in patients with cancer. However, currently available therapeutic approaches still have limited therapeutic effects. Thus, in the past few decades, considerable efforts have been made to discover prospective methods for the treatment of tumor metastasis. The relationships between the chemokine network and tumor metastasis have been reported by numerous studies. Importantly, the CXCL12/CXCR4 axis has drawn substantial attention because CXCR4 is the most common chemokine receptor expressed on tumor cells (2). Previous studies revealed that the CXCL12/CXCR4 axis is responsible for lung, bone marrow, and liver metastasis in a variety of types of cancers (23). Moreover, the CCL21/CCR7 axis (2, 24) and CCL2-CCR2 have also been reported to act as contributors to metastasis (25). In the current study, it was shown that CXCL13 is able to recruit CXCR5$^+$ B cells to metastatic sites, and B cells could secrete IL-10 to inhibit an effective antitumor immune response, which facilitates pulmonary metastasis.

B cells are involved in multiple immunological processes such as the secretion of Igs, Ag presentation, and immunosuppression. B cells that secrete IL-10 are generally considered to be regulatory B cells. However, there is no generally accepted marker Ab panel for the characterization of regulatory B cells. Thus, more investigations are needed for the further understanding and characterization of regulatory B cells. In our study, the regulatory B cells in pulmonary metastasis sites are CD45$^+$CD19$^+$IL-10$^+$CD1d$^+$CD5$^+$CD24^{hi}MHC-II^{hi} B220^{hi}, which have some common features as the reported ones. Moreover, our study has shown that B cell–derived IL-10 could inhibit effective antitumor responses by affecting immune cells in the tumor microenvironment. The reduction of IL-10–producing B cells enhanced antitumor immunity, increased the amount of activated Th and cytotoxic T cells that infiltrated into metastatic sites, and led to the elevation of CD8$^+$ cell–derived IFN-γ. In addition, we found that the mRNA level of granzyme B, IFN-γ, and perforin were increased whereas the mRNA level of TGF-β was reduced. To confirm that IL-10 secreted by regulatory B cells contributes to the development of pulmonary metastasis, we performed adoptive transfer of IL-10–producing B cells or *IL-10*$^{-/-}$ B cells to pulmonary metastasis models established in WT mice. It was shown that the transfer of IL-10–producing B cells led to the inhibition of antitumor immunity and increased the proportion of protumor CD4$^+$Foxp3$^+$ regulatory T cells in metastatic sites.

The relationship between CXCL13 and cancer advancing has been reported by previous studies. The role of CXCL13 on the development of tumors is still controversial. It was reported that the

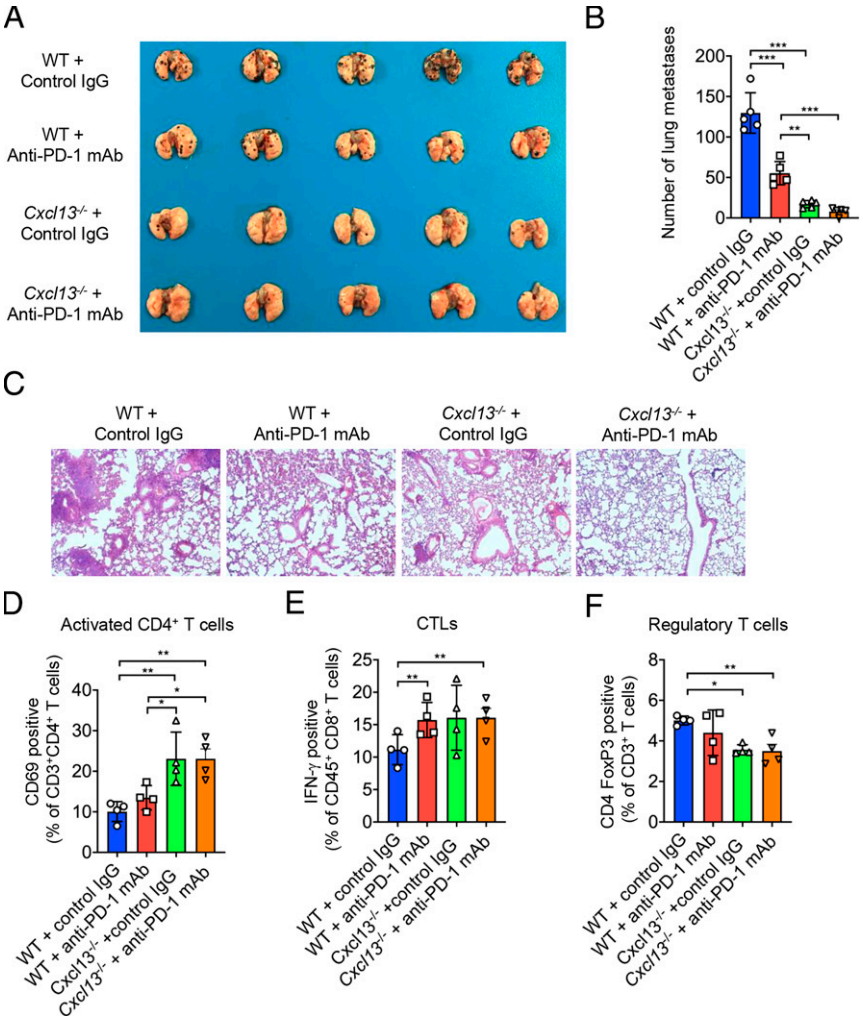

FIGURE 6. Deletion of CXCL13 enhanced the efficacy of cancer immunotherapy targeting PD-1. (**A**) WT and *Cxcl113*$^{-/-}$ mice in treatment groups were i.p. administered with anti–PD-1 mAbs (250 μg/mouse) on days 0 and 3 following i.v. injection of B16-F10 cells (2×10^5). WT and *Cxcl113*$^{-/-}$ mice in control groups were i.p. administered with the same dose of isotype control IgG at the same time points. All mice were sacrificed on day 14 and the gross appearance of the lungs was examined (n = 5 mice). (**B** and **C**) Lungs from WT and *Cxcl113*$^{-/-}$ mice in (A) were isolated for measuring lung metastases of the tumor (B), and lungs were paraffin embedded and stained with H&E (C) (n = 5 mice). Original magnification ×100. (**D**) Single-cell suspension of pulmonary metastatic tumor from mice in (A) were subjected to FCM analysis. The activated $CD4^+$ T cells ($CD4^+$ $CD69^+$) in the tumor metastatic microenvironment were quantified and plotted as a percentage of $CD3^+CD4^+$ T cells (n = 4 mice). (**E**) IFN-γ^+ $CD8^+$ T cells in the tumor metastatic microenvironment were quantified and plotted as a percentage of $CD3^+CD8^+$ T cells ($n = 4$ mice). (**F**) Regulatory T cells ($CD4^+Foxp3^+$) in the tumor metastatic microenvironment were quantified and plotted as a percentage of $CD3^+$ T cells ($n = 4$ mice). Data are presented as mean ± SD. Statistical significance was determined by one-way ANOVA. $*p < 0.05$. $**p < 0.01$. $***p < 0.001$.

deletion of CXCL13 in patients with colorectal tumors is associated with a reduced density of B cells in the invasive margin of tumors, which significantly increased the risks of relapse (3). In addition, CXCL13 has been considered as an important marker for the formation of tertiary lymphoid structures (4), whose crucial roles in the maintenance of the immune-responsive tumor microenvironment was recently revealed (5). Nevertheless, CXCL13 derived from myofibroblasts could promote the progression of malignant prostate cancer (26), and CXCL13 derived from human bone marrow endothelial cells could induce the invasion of prostate cancer cells to bone (27, 38). It has also been observed that in breast cancer and lung cancer patients, the concentrations of CXCL13 in the serum and cancer specimens are increased (29, 30). We speculated that the controversial roles of CXCL13 might be mediated by different mechanisms. The results from the current study suggest that CXCL13 contributes to tumor metastasis through affecting the recruitment of regulatory B cells. However, further studies are needed to completely uncover the influence of CXCL13 on the metastatic immune microenvironment. Moreover, few studies have focused on the chemoresistance and immune-inhibitory properties concerned with CXCL13 expression in tumor treatment. In the current study, we evaluated the therapeutic effects of CTX or Abs targeting PD-1 in *Cxcl13*$^{-/-}$ mice and WT mice. The therapeutic effects of chemotherapy and checkpoint-based immunotherapy were both significantly increased in the pulmonary tumor metastasis model of *Cxcl13*$^{-/-}$ mice when compared with those of the WT control. These results indicated that targeted therapies against CXCL13 or IL-10–producing B cells might be a promising therapeutic strategy to enhance the efficacies of traditional chemotherapy or immunotherapy against advanced pulmonary cancer metastasis.

Disclosures

The authors have no financial conflicts of interest.

References

1. Kitamura, T., B.-Z. Qian, and J. W. Pollard. 2015. Immune cell promotion of metastasis. *Nat. Rev. Immunol.* 15: 73–86.
2. Zlotnik, A., A. M. Burkhardt, and B. Homey. 2011. Homeostatic chemokine receptors and organ-specific metastasis. *Nat. Rev. Immunol.* 11: 597–606.
3. Bindea, G., B. Mlecnik, M. Tosolini, A. Kirilovsky, M. Waldner, A. C. Obenauf, H. Angell, T. Fredriksen, L. Lafontaine, A. Berger, et al. 2013. Spatiotemporal dynamics of intratumoral immune cells reveal the immune landscape in human cancer. *Immunity* 39: 782–795.
4. Dieu-Nosjean, M.-C., J. Goc, N. A. Giraldo, C. Sautès-Fridman, and W. H. Fridman. 2014. Tertiary lymphoid structures in cancer and beyond. *Trends Immunol.* 35: 571–580.
5. Cabrita, R., M. Lauss, A. Sanna, M. Donia, M. Skaarup Larsen, S. Mitra, I. Johansson, B. Phung, K. Harbst, J. Vallon-Christersson, et al. 2020. Tertiary lymphoid structures improve immunotherapy and survival in melanoma. [Published erratum appears in 2020 *Nature* 580: E1.]*Nature* 577: 561–565.
6. Chen, X., Y. Takemoto, H. Deng, M. Middelhoff, R. A. Friedman, T. H. Chu, M. J. Churchill, Y. Ma, K. K. Nagar, Y. H. Tailor, et al. 2017. Histidine decarboxylase (HDC)-expressing granulocytic myeloid cells induce and recruit $Foxp3^+$ regulatory T cells in murine colon cancer. *OncoImmunology* 6: e1290034.
7. Duan, Z., J. Gao, L. Zhang, H. Liang, X. Huang, Q. Xu, Y. Zhang, T. Shen, and F. Lu. 2015. Phenotype and function of $CXCR5^+CD45RA^-CD4^+$ T cells were

altered in HBV-related hepatocellular carcinoma and elevated serum CXCL13 predicted better prognosis. *Oncotarget* 6: 44239–44253.
8. Rempenault, C., J. Mielle, K. Schreiber, P. Corbeau, L. Macia, B. Combe, J. Morel, C. I. Daien, and R. Audo. 2021. CXCR5/CXCL13 pathway, a key driver for migration of regulatory B10 cells, is defective in patients with rheumatoid arthritis. *Rheumatology*. DOI: 10.1093/rheumatology/keab639.
9. Zhu, Q., K. Rui, S. Wang, and J. Tian. 2021. Advances of regulatory B cells in autoimmune diseases. *Front. Immunol.* 12: 592914.
10. Olkhanud, P. B., B. Damdinsuren, M. Bodogai, R. E. Gress, R. Sen, K. Wejksza, E. Malchinkhuu, R. P. Wersto, and A. Biragyn. 2011. Tumor-evoked regulatory B cells promote breast cancer metastasis by converting resting $CD4^+$ T cells to T-regulatory cells. *Cancer Res.* 71: 3505–3515.
11. Shalapour, S., J. Font-Burgada, G. Di Caro, Z. Zhong, E. Sanchez-Lopez, D. Dhar, G. Willimsky, M. Ammirante, A. Strasner, D. E. Hansel, et al. 2015. Immunosuppressive plasma cells impede T-cell-dependent immunogenic chemotherapy. *Nature* 521: 94–98.
12. Meijer, J., I. S. Zeelenberg, B. Sipos, and E. Roos. 2006. The CXCR5 chemokine receptor is expressed by carcinoma cells and promotes growth of colon carcinoma in the liver. *Cancer Res.* 66: 9576–9582.
13. Steele, C. W., S. A. Karim, J. D. G. Leach, P. Bailey, R. Upstill-Goddard, L. Rishi, M. Foth, S. Bryson, K. McDaid, Z. Wilson, et al. 2016. CXCR2 inhibition profoundly suppresses metastases and augments immunotherapy in pancreatic ductal adenocarcinoma. *Cancer Cell* 29: 832–845.
14. Inoue, S., W. W. Leitner, B. Golding, and D. Scott. 2006. Inhibitory effects of B cells on antitumor immunity. *Cancer Res.* 66: 7741–7747.
15. Mizoguchi, A., and A. K. Bhan. 2006. A case for regulatory B cells. *J. Immunol.* 176: 705–710.
16. Shen, P., T. Roch, V. Lampropoulou, R. A. O'Connor, U. Stervbo, E. Hilgenberg, S. Ries, V. D. Dang, Y. Jaimes, C. Daridon, et al. 2014. IL-35-producing B cells are critical regulators of immunity during autoimmune and infectious diseases. *Nature* 507: 366–370.
17. Balkwill, F., A. Montfort, and M. Capasso. 2013. B regulatory cells in cancer. *Trends Immunol.* 34: 169–173.
18. Ni, L., Y. Zheng, M. Hara, D. Pan, and X. Luo. 2015. Structural basis for Mob1-dependent activation of the core Mst-Lats kinase cascade in Hippo signaling. *Genes Dev.* 29: 1416–1431.
19. Affara, N. I., B. Ruffell, T. R. Medler, A. J. Gunderson, M. Johansson, S. Bornstein, E. Bergsland, M. Steinhoff, Y. Li, Q. Gong, et al. 2014. B cells regulate macrophage phenotype and response to chemotherapy in squamous carcinomas. *Cancer Cell* 25: 809–821.
20. Padmanee, S., and J. P. Allison. 2015. The future of immune checkpoint therapy. *Science* 348: 56–61.
21. Robert, C., J. Schachter, G. V. Long, A. Arance, J. J. Grob, L. Mortier, A. Daud, M. S. Carlino, C. McNeil, M. Lotem, et al.; KEYNOTE-006 investigators. 2015. Pembrolizumab versus ipilimumab in advanced melanoma. *N. Engl. J. Med.* 372: 2521–2532.
22. Larkin, J., V. Chiarion-Sileni, R. Gonzalez, J. J. Grob, C. L. Cowey, C. D. Lao, D. Schadendorf, R. Dummer, M. Smylie, P. Rutkowski, et al. 2015. Combined nivolumab and ipilimumab or monotherapy in untreated melanoma. *N. Engl. J. Med.* 373: 23–34.
23. Li, Y. M., Y. Pan, Y. Wei, X. Cheng, B. P. Zhou, M. Tan, X. Zhou, W. Xia, G. N. Hortobagyi, D. Yu, and M. C. Hung. 2004. Upregulation of CXCR4 is essential for HER2-mediated tumor metastasis. *Cancer Cell* 6: 459–469.
24. Wiley, H. E., E. B. Gonzalez, W. Maki, M. T. Wu, and S. T. Hwang. 2001. Expression of CC chemokine receptor-7 and regional lymph node metastasis of B16 murine melanoma. *J. Natl. Cancer Inst.* 93: 1638–1643.
25. Qian, B. Z., J. Li, H. Zhang, T. Kitamura, J. Zhang, L. R. Campion, E. A. Kaiser, L. A. Snyder, and J. W. Pollard. 2011. CCL2 recruits inflammatory monocytes to facilitate breast-tumour metastasis. *Nature* 475: 222–225.
26. Massimo, A., S. Shalapour, Y. Kang, C. A. M. Jamieson, and M. Karin. 2014. Tissue injury and hypoxia promote malignant progression of prostate cancer by inducing CXCL13 expression in tumor myofibroblasts. *Proc. Natl. Acad. Sci. USA* 111: 14776–14781.
27. Singh, S., R. Singh, P. K. Sharma, U. P. Singh, S. N. Rai, L. W. Chung, C. R. Cooper, K. R. Novakovic, W. E. Grizzle, and J. W. Lillard, Jr. 2009. Serum CXCL13 positively correlates with prostatic disease, prostate-specific antigen and mediates prostate cancer cell invasion, integrin clustering and cell adhesion. *Cancer Lett.* 283: 29–35.
28. El Haibi, C. P., P. K. Sharma, R. Singh, P. R. Johnson, J. Suttles, S. Singh, and J. W. Lillard, Jr. 2010. PI3Kp110-, Src-, FAK-dependent and DOCK2-independent migration and invasion of CXCL13-stimulated prostate cancer cells. *Mol. Cancer* 9: 85.
29. Panse, J., K. Friedrichs, A. Marx, Y. Hildebrandt, T. Luetkens, K. Barrels, C. Horn, T. Stahl, Y. Cao, K. Milde-Langosch, et al. 2008. Chemokine CXCL13 is overexpressed in the tumour tissue and in the peripheral blood of breast cancer patients. *Br. J. Cancer* 99: 930–938.
30. Wang, G. Z., X. Cheng, B. Zhou, Z. S. Wen, Y. C. Huang, H. B. Chen, G. F. Li, Z. L. Huang, Y. C. Zhou, L. Feng, et al. 2015. The chemokine CXCL13 in lung cancers associated with environmental polycyclic aromatic hydrocarbons pollution. *eLife* 4: e09419.